Vitrification and determination of the crystallization time scales of the bulk-metallic-glass-forming liquid $Zr_{58.5}Nb_{2.8}Cu_{15.6}Ni_{12.8}Al_{10.3}$

C. C. Hays,[a] J. Schroers, and W. L. Johnson
Division of Engineering and Applied Science, California Institute of Technology, Pasadena, California 91125

T. J. Rathz
University of Alabama at Huntsville, Huntsville, Alabama 35899

R. W. Hyers, J. R. Rogers, and M. B. Robinson
NASA Marshall Space Flight Center, Huntsville, Alabama 35812

(Received 23 April 2001; accepted for publication 1 July 2001)

The crystallization kinetics of $Zr_{58.5}Nb_{2.8}Cu_{15.6}Ni_{12.8}Al_{10.3}$ were studied in an electrostatic levitation (ESL) apparatus. The measured critical cooling rate is 1.75 K/s. $Zr_{58.5}Nb_{2.8}Cu_{15.6}Ni_{12.8}Al_{10.3}$ is the first bulk-metallic-glass-forming liquid that does not contain beryllium to be vitrified by purely radiative cooling in the ESL. Furthermore, the sluggish crystallization kinetics enable the determination of the time-temperature-transformation (TTT) diagram between the liquidus and the glass transition temperatures. The shortest time to reach crystallization in an isothermal experiment; i.e., the nose of the TTT diagram is 32 s. The nose of the TTT diagram is at 900 K and positioned about 200 K below the liquidus temperature. © *2001 American Institute of Physics.* [DOI: 10.1063/1.1398605]

The discovery of Zr-based bulk-metallic glasses has triggered tremendous research activity. There are a limited number of the multicomponent bulk-metallic-glass-forming alloy systems; e.g., Zr–Ti–Cu–Ni–Be (Ref. 1), Zr–Al–Cu–Ni (Ref. 2), Zr–Nb–Cu–Ni–Al (Ref. 3) and Zr–Ti–Cu–Ni.[4] The critical cooling rate required to vitrify *ideal* alloys in the respective composition manifolds varies from 1.8 K/s in Zr–Ti–Cu–Ni–Be, to 10^2 K/s in the quaternary Zr–Ti–Cu–Ni system. Electrostatic levitation (ESL) and calorimetric methods have examined in detail the crystallization behavior of one of the beryllium containing bulk-metallic glasses, $Zr_{41.2}Ti_{13.8}Cu_{12.5}Ni_{10}Be_{22.5}$.[5,6] Recently, a composition in the Zr–Nb–Cu–Ni–Al system has been found that appears to have an excellent glass forming ability.[7] Measurements on the alloy $Zr_{58.5}Nb_{2.8}Cu_{15.6}Ni_{12.8}Al_{10.3}$ have shown that it can be vitrified via conventional processing techniques; e.g., arc melting. With a critical casting thickness of greater than 1.5 cm, the expected critical cooling rate should be less than 10 K/s. This low cooling rate motivated our studies of this composition in the ESL. The ESL provides an ideal platform for the study of liquid metals in the metastable undercooled liquid region.[8] This letter reports crystallization studies in the undercooled liquid state of $Zr_{58.5}Nb_{2.8}Cu_{15.6}Ni_{12.8}Al_{10.3}$ obtained via processing in the ESL. Constant cooling experiments are presented that determine the critical cooling rate required to vitrify the material. Furthermore, the entire time-temperature-transformation (TTT) diagram was determined, and allows for the interpretation of the crystallization kinetics of this bulk glass-forming alloy under isothermal conditions.

The $Zr_{58.5}Nb_{2.8}Cu_{15.6}Ni_{12.8}Al_{10.3}$ ESL specimens were prepared from high purity elements via arc melting in an ultrahigh purity Ar atmosphere. Figure 1 shows a differential scanning calorimetry measurement conducted with a heating rate of 20 K/min on a mg-sized ESL specimen. The glass transition is observed at $T_g = 674$ K, followed by primary crystallization at $T_x = 776$ K. The supercooled liquid region (SLR) interval is $\Delta T = T_x - T_g = 102$ K. ESL specimens, 30–45 mg in mass, were cut from 25 g mass ingots. The 25 g ingots were vitrified on cooling in the arc furnace, each approximately 1.5 cm thick.

Figure 2 shows free and rate-controlled cooling curves for a $Zr_{58.5}Nb_{2.8}Cu_{15.6}Ni_{12.8}Al_{10.3}$ ESL specimen. Curve 2(**c**)

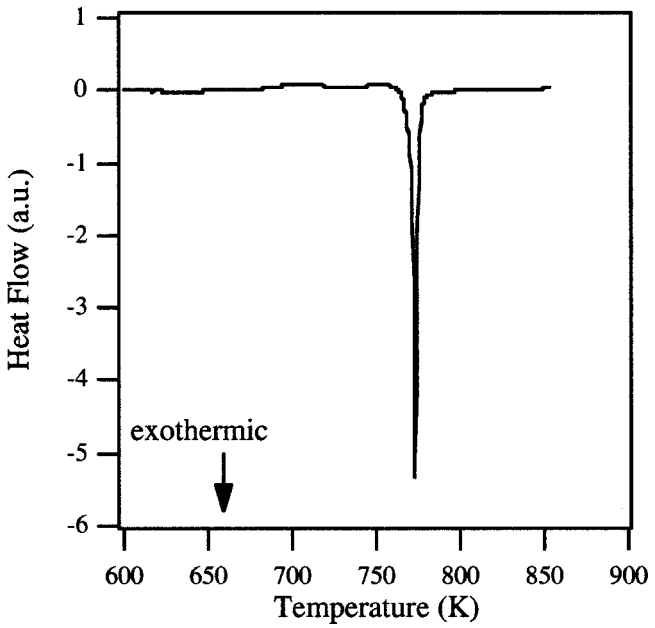

FIG. 1. Differential scanning calorimetry thermogram of $Zr_{58.5}Nb_{2.8}Cu_{15.6}Ni_{12.8}Al_{10.3}$ is shown. Glass transition temperature is 674 K, with primary crystallization at 776 K, when heated at 20 K/min.

[a]Author to whom all correspondence should be addressed; electronic mail: chays@hyperfine.caltech.edu

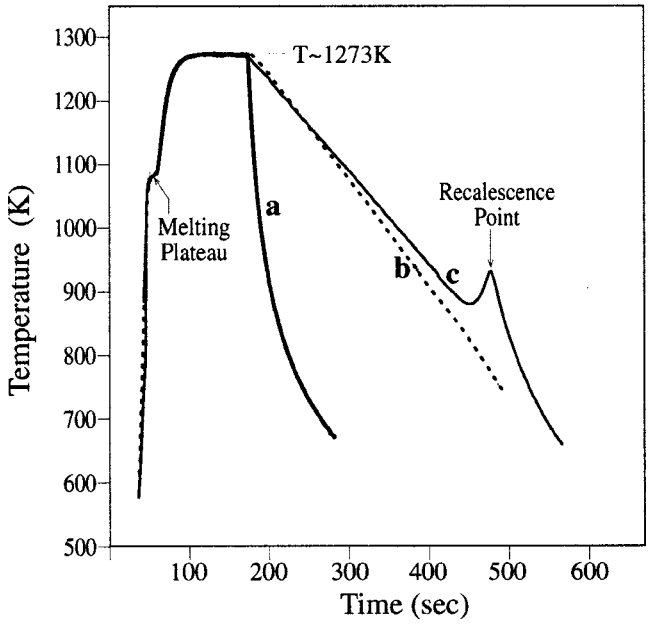

FIG. 2. Cooling curves for $Zr_{58.5}Nb_{2.8}Cu_{15.6}Ni_{12.8}Al_{10.3}$: (**a**)—free cooling, (**b**)—controlled cooling at 1.75 K/s, and (**c**)—controlled cooling at 1.5 K/s are shown.

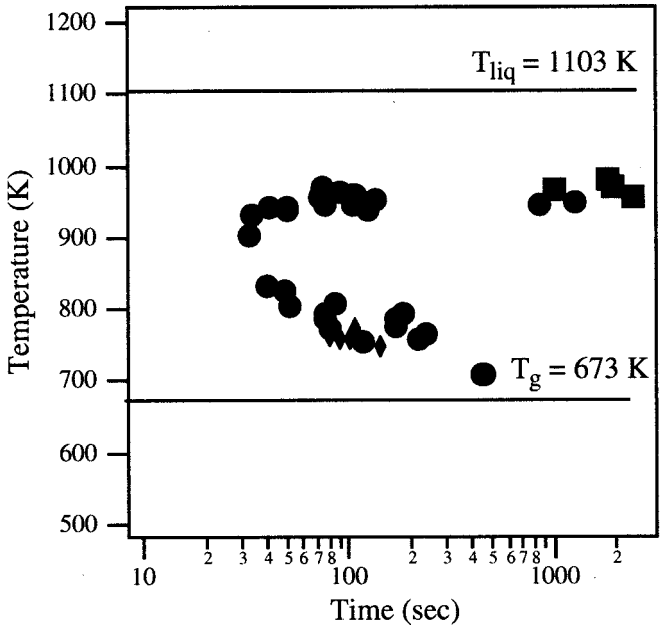

FIG. 3. Experimental $Zr_{58.5}Nb_{2.8}Cu_{15.6}Ni_{12.8}Al_{10.3}$ the TTT diagram is shown. Circles and squares denote data collected on cooling from the liquid state to an isothermal temperature. Diamonds depict data collected on heating from the amorphous state.

shows the onset of crystallization at ≈880 K upon constant cooling at 1.5 K/s. Crystallization is manifest by a recalescence event; i.e., the reheating of the specimen due to the release of the heat of fusion. Cooling at 1.75 K/s [curve 2(**b**)] is sufficient to circumvent detectable crystallization and therefore vitrify the material. Curve 2(**a**) represents a free cooling curve, and a corresponding maximum cooling rate of 5–10 K/s in the critical temperature range near ≈800 K. In order to prove that the sample of curve 2(**b**) was vitrified upon cooling, following cooling the specimen was heated at ≈20 K/min. Crystallization was observed at $T_x \approx 774$ K, thus verifying the glassy condition.

Prior to isothermal experiments, specimens were heated to 1273 K, held for 60 s, and then cooled to the desired isothermal temperature. The results of these isothermal crystallization studies, performed between the liquidus and glass transition temperatures are summarized in the $Zr_{58.5}Nb_{2.8}Cu_{15.6}Ni_{12.8}Al_{10.3}$ TTT diagram depicted in Fig. 3, which shows the time to reach crystallization for a given isothermal temperature. Strictly speaking, the radiative cooling time to reach the plateau cannot be neglected in comparison to the elapsed time at the plateau temperature. As such, the diagram determined is not a quantitative TTT diagram. On the other hand, the radiative cooling segment (≈20 s) is identical for all undercooling cycles so that the effect is systematic for all cycles. The data define a well-developed nose, $(T_{nose}, t_{nose}) \approx$(900 K, 32 s) which has also been observed in $Zr_{41.2}Ti_{13.8}Cu_{12.5}Ni_{10}Be_{22.5}$ and Pd-based alloys.[9,10] The nose of the TTT diagram is positioned about 200 K below the liquidus temperature. Between 900–1000 K, and near 700 K, the liquid could be held for >30 min without recalescence. Subsequent cooling at 2 K/s vitrified the liquid (square data points of Fig. 3). Therefore, the square data points give a lower bound for the crystallization time. Above the nose of the curve there is relatively little scatter in the crystallization onset times. This behavior is different from what has been observed in the bulk glass formers previously mentioned (Refs. 9 and 10). In $Zr_{41.2}Ti_{13.8}Cu_{12.5}Ni_{10}Be_{22.5}$ and $Pd_{43}Cu_{27}Ni_{10}P_{20}$, a large scatter in the time to reach crystallization above the nose of the TTT diagram was explained by a nucleation controlled crystallization mechanism.

In Fig. 3, at low temperatures just above T_g, no difference in the time to reach crystallization were observed (diamond data points of Fig. 3), on cooling from the liquid state or heating the vitrified material into the isothermal plateau. However in $Zr_{41.2}Ti_{13.8}Cu_{12.5}Ni_{10}Be_{22.5}$, as the isothermal temperature increases towards the nose of the TTT diagram, a large asymmetry for crystallization, on heating versus cooling, sets in.[11] Thus, we performed rapid heating experiments in the ESL on $Zr_{58.5}Nb_{2.8}Cu_{15.6}Ni_{12.8}Al_{10.3}$ specimens. Heating at rates up to 500 K/s still lead to crystallization suggesting an asymmetry of at least two orders of magnitude in the critical cooling and critical heating rates. The explanation for this asymmetry is given by the fact that in metallic systems, the maximum in the nucleation rate is always at a lower temperature than the maximum in the crystal growth rate. This results in different critical heating and cooling rates. Nuclei formed upon cooling at the maximum in the nucleation rate experience a low growth rate, whereas nuclei formed at the nose of the TTT diagram upon heating are exposed to the maximum growth rate. A similar behavior has been observed in $Zr_{41.2}Ti_{13.8}Cu_{12.5}Ni_{10}Be_{22.5}$.[12]

The data of Fig. 3 represent a seminal example of the TTT diagram for a bulk-metallic-glass-forming liquid. The crystallization kinetics of $Zr_{58.5}Nb_{2.8}Cu_{15.6}Ni_{12.8}Al_{10.3}$ are comparable to the beryllium containing glass, $Zr_{41.2}Ti_{13.8}Cu_{12.5}Ni_{10}Be_{22.5}$, developed by Peker *et al.*[1] The nose of the $Zr_{41.2}Ti_{13.8}Cu_{12.5}Ni_{10}Be_{22.5}$ TTT diagram was observed at 900 K and 48 s, which is located about 100 K below the liquidus temperature. The TTT diagrams for hese two alloys are quite similar, and indicate that the main underlying physical mechanisms of crystallization might be common in origin. The nose of the

$Zr_{58.5}Nb_{2.8}Cu_{15.6}Ni_{12.8}Al_{10.3}$ TTT diagram occurs at an undercooling roughly twice that of $Zr_{41.2}Ti_{13.8}Cu_{12.5}Ni_{10}Be_{22.5}$, 200 K vs 100 K, respectively. The driving force for crystallization increases with decreasing temperature, while at the same time the atomic mobility decreases with temperature. The differing temperature dependence of these two contributions is manifest in the shape of the TTT diagram nose. This suggests that for $Zr_{58.5}Nb_{2.8}Cu_{15.6}Ni_{12.8}Al_{10.3}$ either, the free energy difference between the liquid and solid is smaller or the atomic mobility is greater than that of $Zr_{41.2}Ti_{13.8}Cu_{12.5}Ni_{10}Be_{22.5}$ given the similarity of the curve positions.

Several criteria are employed in the development of bulk metallic glasses; e.g., compositions are close to deep eutectics, and often exhibit large reduced glass transition temperatures, T_{rg}, where T_{rg} is the ratio of the glass transition temperature, T_g, to the liquidus temperature, T_{liq}. They exhibit a high resistance to crystallization, manifest by large SLR values. $Zr_{58.5}Nb_{2.8}Cu_{15.6}Ni_{12.8}Al_{10.3}$ is the lowest melting composition observed, to date, in this region of the composition manifold. Following Turnbull, glasses with critical cooling rates of $R_C \approx 1$ K/s whether polymeric or ceramic, often exhibit a value of $T_{rg} \approx 2/3$.[13] From Fig. 2, the critical cooling rate for $Zr_{58.5}Nb_{2.8}Cu_{15.6}Ni_{12.8}Al_{10.3}$ is $R_C = 1.75$ K/s. This low value is contrasted by a modest $T_{rg} = 673\,\text{K}/1103\,\text{K} = 0.61$. Again, from the Turnbull criteria, this low $T_{rg} = 0.61$ is indicative of a poor glass-forming ability; i.e., with $R_C = 1.75$ K/s, we might expect a T_{rg} closer to 2/3. Indeed, for $Zr_{41.2}Ti_{13.8}Cu_{12.5}Ni_{10}Be_{22.5}$ $T_{rg} = 0.62 = 623\,\text{K}/1026\,\text{K}$. Thus, the Turnbull criteria cannot explain the excellent glass-forming ability in these systems. $Zr_{58.5}Nb_{2.8}Cu_{15.6}Ni_{12.8}Al_{10.3}$ also exhibits a large SLR, with $\Delta T = 102$ K. However, this is not a necessary condition for good bulk glass formation. Recent work by Waniuk *et al.* on the beryllium-containing alloys first reported by Hays *et al.* show that the critical cooling rate, and the SLR width, have an inverse trend.[14,15] The SLR width is indicative of what are now known to be diffusion-controlled crystallization mechanisms, as opposed to the nucleation controlled crystallization mechanisms active above the nose of the TTT diagram.

We have previously shown that a neighboring composition of the investigated alloy, $Zr_{57}Nb_5Cu_{15.4}Ni_{12.6}Al_{10}$, has a TTT diagram which is comprised of two branches.[16] Indicating that two independent nucleation mechanisms limit the glass forming ability of this composition, which could not be vitrified on free cooling in the ESL. Indeed, a large scatter in the onset times to crystallization at high temperatures for this composition were observed, and related to the crossing of the high temperature branches. In fact, the $Zr_{58.5}Nb_{2.8}Cu_{15.6}Ni_{12.8}Al_{10.3}$ TTT diagram of Fig. 3 qualitatively represents what we referred to previously as the high temperature branch of the $Zr_{57}Nb_5Cu_{15.4}Ni_{12.6}Al_{10}$ TTT diagram. Together, these results indicate that the solubility limits, and resultant topological instability, of the crystalline phases that compete with the glassy state may be controlled over quite narrow ranges in composition. The quantitative aspects of these phenomena are the subject of upcoming publications.

In conclusion, $Zr_{58.5}Nb_{2.8}Cu_{15.6}Ni_{12.8}Al_{10.3}$ is the first bulk-metallic-glass-forming liquid that does not contain beryllium to be vitrified by purely radiative Stefan–Boltzmann cooling in the electrostatic levitator. The critical cooling rate required to vitrify this composition is 1.75 K/s. In addition, we have determined the TTT diagram for this alloy, and this diagram provides alternate insights regarding the crystallization mechanisms active in bulk-glass-forming liquids.

The authors acknowledge the support of the National Aeronautics and Space Administration (Grant No. NAG8-1744) and the Department of Energy (Grant No. DEFG-03-86ER45242). Portions of this work were carried out in the electrostatic levitation facility at the NASA Marshall Space Flight Center, Huntsville, AL. The authors thank Bob Turring of Caltech's Graphics Arts Department.

[1] A. Peker and W. L. Johnson, Appl. Phys. Lett. **63**, 2342 (1993).
[2] T. Zhang, A. Inoue, and T. Masumoto, Mater. Trans., JIM **32**, 1005 (1991).
[3] X. H. Lin, Ph.D. dissertation, California Institute of Technology (1997).
[4] X. H. Lin and W. L. Johnson, J. Appl. Phys. **78**, 6514 (1995).
[5] Y. J. Kim, R. Busch, W. L. Johnson, A. J. Rulison, and W. K. Rhim, Appl. Phys. Lett. **68**, 1057 (1996).
[6] T. A. Waniuk, R. Busch, A. Masuhr, and W. L. Johnson, Acta Mater. **46**, 5229 (1998).
[7] C. C. Hays, J. Schroers, U. Geyer, S. Bossuyt, N. Stein, and W. L. Johnson, J. Metastable and Nanocryst. Mater. **8**, 103 (2000).
[8] W.-K. Rhim, S. K. Chung, D. Barber, K. F. Man, G. Gutt, A. J. Rulison, and R. E. Spjut, Rev. Sci. Instrum. **64**, 2961 (1993).
[9] J. Schroers, R. Busch, and W. L. Johnson, Appl. Phys. Lett. **76**, 2343 (2000).
[10] J. Schroers, Y. Wu, R. Busch, and W. L. Johnson, Acta Mater. (in press).
[11] J. Schroers, R. Busch, A. Masuhr, and W. L. Johnson, Phys. Rev. B **60**, 11855 (1999).
[12] J. Schroers, R. Busch, S. Bossuyt, and W. L. Johnson, Mat. Sci. Eng., 14029 (2000).
[13] D. Turnbull, Contemp. Phys. **10**, 473 (1969).
[14] C. C. Hays, C. P. Kim, and W. L. Johnson, Appl. Phys. Lett. **75**, 1089 (1999).
[15] T. A. Waniuk, J. Schroers, and W. L. Johnson, Appl. Phys. Lett. **78**, 1213 (2001).
[16] C. C. Hays, J. Schroers, D. S. Lee, and W. L. Johnson, NASA Microgravity Workshop, Proc. Metals, Minerals & Materials Society, San Diego, CA, 1998).